Received: 10 March 2020 | Revised: 28 October 2020 | Accepted: 2 November 2020

DOI: 10.1111/mmi.14639

RESEARCH ARTICLE

WILEY

Novel Fus3- and Ste12-interacting protein FsiA activates cell fusion-related genes in both Ste12-dependent and -independent manners in Ascomycete filamentous fungi

Takuya Katayama[1,2] | Özgür Bayram[3] | Taoning Mo[1] | Betim Karahoda[3] | Oliver Valerius[4] | Daigo Takemoto[5] | Gerhard H. Braus[4] | Katsuhiko Kitamoto[6] | Jun-ichi Maruyama[1,2]

[1]Department of Biotechnology, The University of Tokyo, Tokyo, Japan

[2]Collaborative Research Institute for Innovative Microbiology, The University of Tokyo, Tokyo, Japan

[3]Biology Department, Maynooth University, Maynooth, Ireland

[4]Department of Molecular Microbiology and Genetics, Institute of Microbiology and Genetics, and Göttingen Center for Molecular Biosciences (GZMB), Georg-August University, Göttingen, Germany

[5]Graduate School of Bioagricultural Sciences, Nagoya University, Nagoya, Japan

[6]Pharmaceutical Medical Business Sciences, Nihon Pharmaceutical University, Tokyo, Japan

Correspondence
Jun-ichi Maruyama, Department of Biotechnology, The University of Tokyo, Bunkyo-ku, Tokyo, Japan.
Email: amarujun@mail.ecc.u-tokyo.ac.jp

Funding information
Japan Society for the Promotion of Science (JSPS) KAKENHI, Grant/Award Number: 18H0212 and JP17K15242; Science Foundation Ireland, Grant/Award Number: 13/CDA/2142

Abstract

Filamentous fungal cells, unlike yeasts, fuse during vegetative growth. The orthologs of mitogen-activated protein (MAP) kinase Fus3 and transcription factor Ste12 are commonly involved in the regulation of cell fusion. However, the specific regulatory mechanisms underlying cell fusion in filamentous fungi have not been revealed. In the present study, we identified the novel protein FsiA as an AoFus3- and AoSte12-interacting protein in the filamentous fungus *Aspergillus oryzae*. The expression of *AonosA* and cell fusion-related genes decreased upon *fsiA* deletion and increased with *fsiA* overexpression, indicating that FsiA is a positive regulator of cell fusion. In addition, the induction of cell fusion-related genes by *fsiA* overexpression was also observed in the *Aoste12* deletion mutant, indicating that FsiA can induce the cell fusion-related genes in an AoSte12-independent manner. Surprisingly, the *fsiA* and *Aoste12* double deletion mutant exhibited higher cell fusion efficiency and increased mRNA levels of the cell fusion-related genes as compared to the *fsiA* single deletion mutant, which revealed that AoSte12 represses the cell fusion-related genes in the *fsiA* deletion mutant. Taken together, our data demonstrate that FsiA activates the cell fusion-related genes by suppressing the negative function of AoSte12 as well as by an AoSte12-independent mechanism.

KEYWORDS

Aspergillus oryzae, cell fusion, filamentous fungi, sclerotia formation, sexual development

1 | INTRODUCTION

Cell fusion is an essential process to create multinucleated cells and is indispensable for various cellular events such as muscle development, formation of giant cells of the macrophage lineage and the fertilization during sexual reproduction in eukaryotic cells (Chen et al., 2007). In the yeasts *Saccharomyces cerevisiae* and *Schizosaccharomyces pombe*, cell fusion occurs between cells of opposite mating types, and the diploid cells formed by cell fusion can undergo sporulation (Merlini et al., 2013). Similarly, cell fusion of filamentous fungi is crucial for sexual development, but also occurs during vegetative growth in a mating type-independent manner (Fleißner et al., 2008), suggesting a different regulation of cell fusion from yeasts.

In *S. cerevisiae*, the regulatory mechanisms of the mating process are well understood: Recognition of pheromone leads to activation of the downstream mitogen-activated protein (MAP) kinase cascade consisting of MAP kinase kinase kinase Ste11, MAP kinase kinase Ste7 and MAP kinase Fus3. Ste5 functions as a scaffold protein for this MAP kinase cascade promoting phosphorylation of

TABLE 1 Proteins detected in the TAP analysis

Locus ID	1st experiment		2nd experiment		Description
	Coverage (%)	Peptides (Hits)	Coverage (%)	Peptides (Hits)	
AO090701000086 (FsiA)	20.04	29	10.76	17	Uncharacterized protein
AO090009000638 (AoSte12)	8.30	7	3.15	3	Ortholog of Ste12p with a predicted role in regulation of transcription

Fus3. Phosphorylated Fus3 in turn activates transcription factor Ste12, which modulates the expression of genes required for mating (Merlini et al., 2013). Fus3 activates Ste12 by directly phosphorylating Ste12 and its inhibitors Dig1/Dig2 (Wong Sak Hoi & Dumas, 2010).

In filamentous fungi, the orthologous components of the Fus3 MAP kinase cascade and Ste12 are highly conserved (Rispail et al., 2009), suggesting a similar signaling pathway to that of yeast. However, as Ste5, Dig1, and Dig2 are not conserved, the regulation of cell fusion by Fus3 and Ste12 orthologs may be different. Fus3 orthologs of filamentous fungi have been involved in various cellular processes such as sexual development, pathogenicity, and secondary metabolism (Li et al., 2005; Paoletti et al., 2007; Priegnitz et al., 2015; Rispail & Di Pietro, 2009; Xu & Hamer, 1996). Importantly, the Fus3 orthologs were shown to be essential for cell fusion in multiple filamentous fungi such as *Neurospora crassa* (Herzog et al., 2015) and *Aspergillus nidulans* (Jun et al., 2011). In contrast to Fus3 orthologs, the functions of Ste12 orthologs in sexual development and cell fusion are not consistent across filamentous fungal species. The deletion mutants of the Ste12 orthologs exhibit no sexual development in *N. crassa* (Li et al., 2005) and *A. nidulans* (Vallim et al., 2000), while the mutants form fruiting bodies without any ascospores in *Sordaria macrospora* (Nolting & Pöggeler, 2006) and exhibits no defects of sexual development in *Magnaporthe grisea* (Park et al., 2002). Similarly, Ste12 orthologs are required for cell fusion in *N. crassa* (Herzog et al., 2015) but not in *Fusarium oxysporum* (Rispail & Di Pietro, 2009). As such varying contributions by Fus3 and Ste12 orthologs cannot be simply explained according to the activation mechanism of Fus3 and Ste12 in *S. cerevisiae*, it is assumed that an unknown related machinery involving additional component exists for the regulation of cell fusion and sexual development in filamentous fungi.

Among filamentous fungi, *N. crassa* is a well-developed model for investigating cell fusion mechanisms due to its high cell fusion efficiency. In *N. crassa*, Ste11 ortholog NRC-1 and Ste7 ortholog MEK-2 are also required for cell fusion along with Fus3 ortholog MAK-2 and Ste12 ortholog PP-1 (Fu et al., 2011; Pandey et al., 2004). PP-1 is predicted to function downstream of MAK-2 because the transcriptome analysis showed a group of genes shared between MAK-2-dependent and PP-1-dependent gene expression (Leeder et al., 2013). Several genes involved in cell fusion such as *ham* (Hyphal Anastomosis Mutant) genes have been identified (Fu et al., 2011; Jonkers et al., 2016), and expression of some *ham* genes is dependent on PP-1 during cell fusion (Leeder et al., 2013). Moreover, PP-1 directly stimulates the expression of *adv-1* encoding another transcription factor, thereby promoting the genes related to cell fusion (Fischer et al., 2018). These findings suggest that MAK-2 activates PP-1, which in turn induces the *ham* genes via *adv-1* expression (Fischer et al., 2018). However, it is unclear how PP-1 is regulated by MAK-2 or other upstream components. In addition, the regulation of cell fusion-related genes has been poorly characterized in filamentous fungi other than *N. crassa*.

Aspergillus oryzae is an industrially important filamentous fungus for Japanese food fermentation and heterologous protein production (Kitamoto, 2002). However, the cell fusion efficiency of *A. oryzae* is much lower than that of *N. crassa*, making the investigation of cell fusion difficult in this fungus. We previously established a method for quantitative measurement of cell fusion by auxotrophic complementation and showed the requirement of Fus3 ortholog AoFus3 for cell fusion in *A. oryzae* (Tsukasaki et al., 2014). In this study, we identified FsiA as a novel protein interacting with AoFus3 and Ste12 ortholog AoSte12 and demonstrated that FsiA positively regulates the cell fusion-related genes in an AoSte12-independent manner. In addition, FsiA displays a suppressive function in the AoSte12-mediated repression, thereby activating the cell fusion-related genes.

2 | RESULTS

2.1 | Identification of AoFus3-interacting proteins by tandem affinity purification

AoFus3 was previously shown to be essential for cell fusion, but its functions in this cellular process have not been determined. To clarify the functions of AoFus3, we performed a tandem affinity purification (TAP) analysis using the strain expressing AoFus3 tagged with a C-terminal TAP-tag. The experiment was performed in duplicate, and peptides from two proteins were commonly detected (Table 1 and Figure S1). One of them was AO090009000638 (AoSte12), an ortholog of Ste12, but the other protein AO090701000086 was uncharacterized. Interestingly, yeast two-hybrid analysis and co-immunoprecipitation revealed AO090701000086-AoSte12 interaction besides the AO090701000086-AoFus3 and AoSte12-AoFus3 interactions (Figure 1), indicating that AO090701000086, AoFus3 and AoSte12 interact with one another. Therefore, we designated AO090701000086 as FsiA (AoFus3 and AoSte12 Interacting).

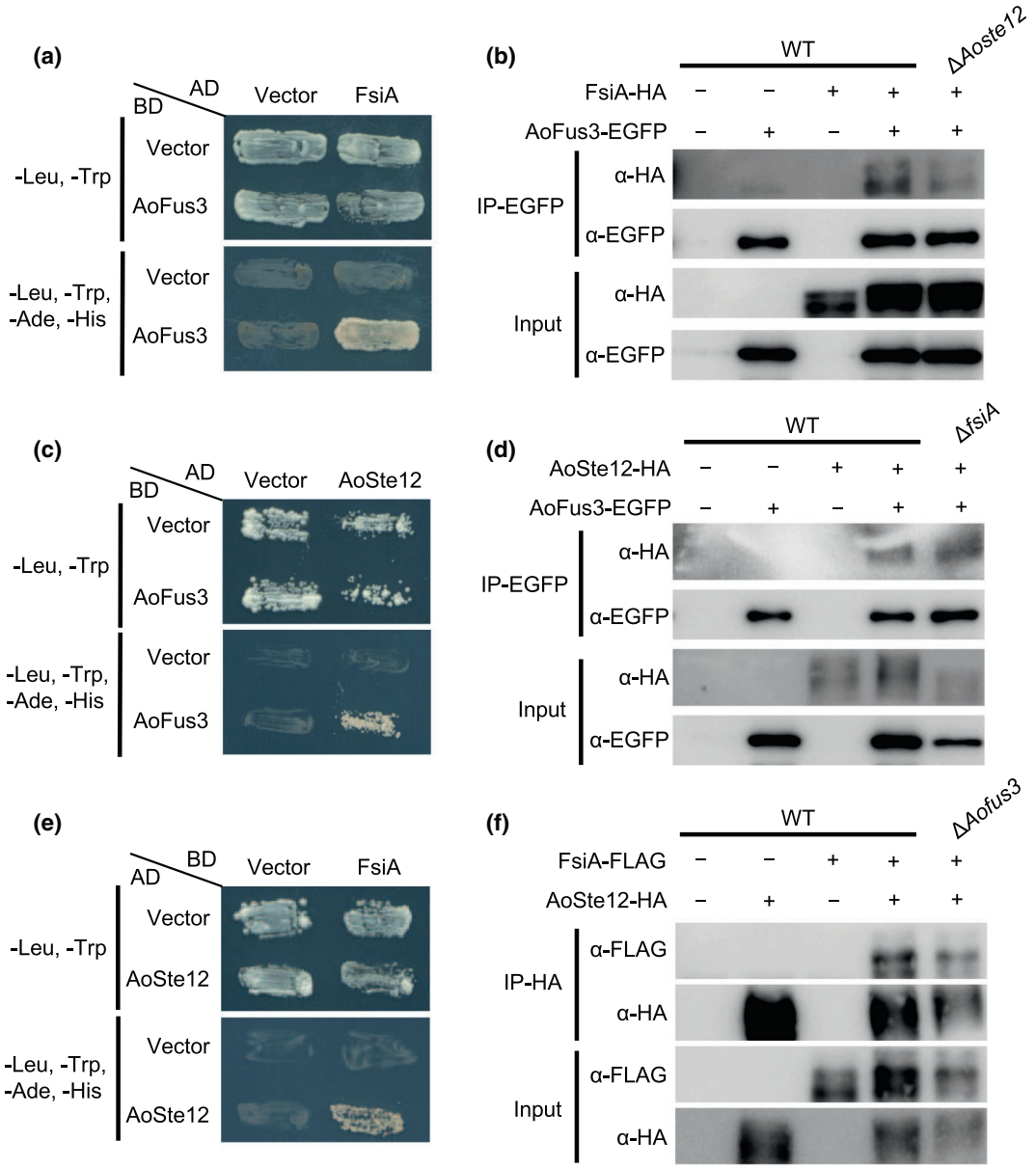

FIGURE 1 Interaction among FsiA, AoFus3, and AoSte12. (a, b, and c) Yeast two hybrid analysis detecting interactions between FsiA-AoFus3 (a), AoFus3-AoSte12 (B), and FsiA-AoSte12 (c). (d, e, and f) Co-immunoprecipitation analysis detecting interactions between FsiA-AoFus3 (d), AoFus3-AoSte12 (e), and FsiA-AoSte12 (f). Cell extracts were prepared from the wild-type strain K1, the *fsiA-HA*-expressing strain K-AfsiAH, the *fsiA-FLAG*-expressing strain K-AfsiAF, the *Aofus3-EGFP*-expressing strainK-Af3G, the *Aoste12-HA*-expressing strain K-As12H, the *fsiA-HA*/*Aofus3-EGFP*-expressing strain K-AfsiAHAf3G, the *fsiA-HA*/*Aofus3-EGFP*-expressing Δ*Aoste12* strain KΔs12-AfsiAHAf3G, the *Aoste12-HA*/*Aofus3-EGFP*-expressing strain K-As12HAf3G, the *Aoste12-HA*/*Aofus3-EGFP*-expressing Δ*fsiA* strain KΔfsiA-As12HAf3G, the *Aoste12-HA*/*fsiA-FLAG*-expressing strain K-As12HAfsiAF and the *Aoste12-HA*/*fsiA-FLAG*-expressing Δ*Aofus3* strain KΔf3-As12HAfsiAF

2.2 | FsiA is involved in growth, conidiation and sclerotia formation, and localizes to nuclei

Rapid amplification of cDNA ends (RACE) analysis revealed that the sequences of exons and an intron of *fsiA* were consistent with the prediction in AspGD (http://www.aspergillusgenome.org) (Figure S2), resulting in a 474 amino acids protein, and phylogenetic analysis showed its specific conservation in Pezizomycotina, a group of filamentous fungal species belonging to Ascomycota, but not in yeasts or other organisms (Figure 2a). Although we attempted to search functional domains using SMART (http://smart.embl-heidelberg.de), no specific domains were found.

To elucidate the function of FsiA, we constructed a *fsiA* deletion mutant as well as an *Aoste12* deletion mutant, and investigated their phenotypes along with the *Aofus3* deletion mutant. The growth of the *Aoste12* deletion mutant slightly increased as compared to the wild-type strain, while the *fsiA* deletion mutant exhibited a more severe growth defect than the *Aofus3* deletion mutant (Figure 2b,c).

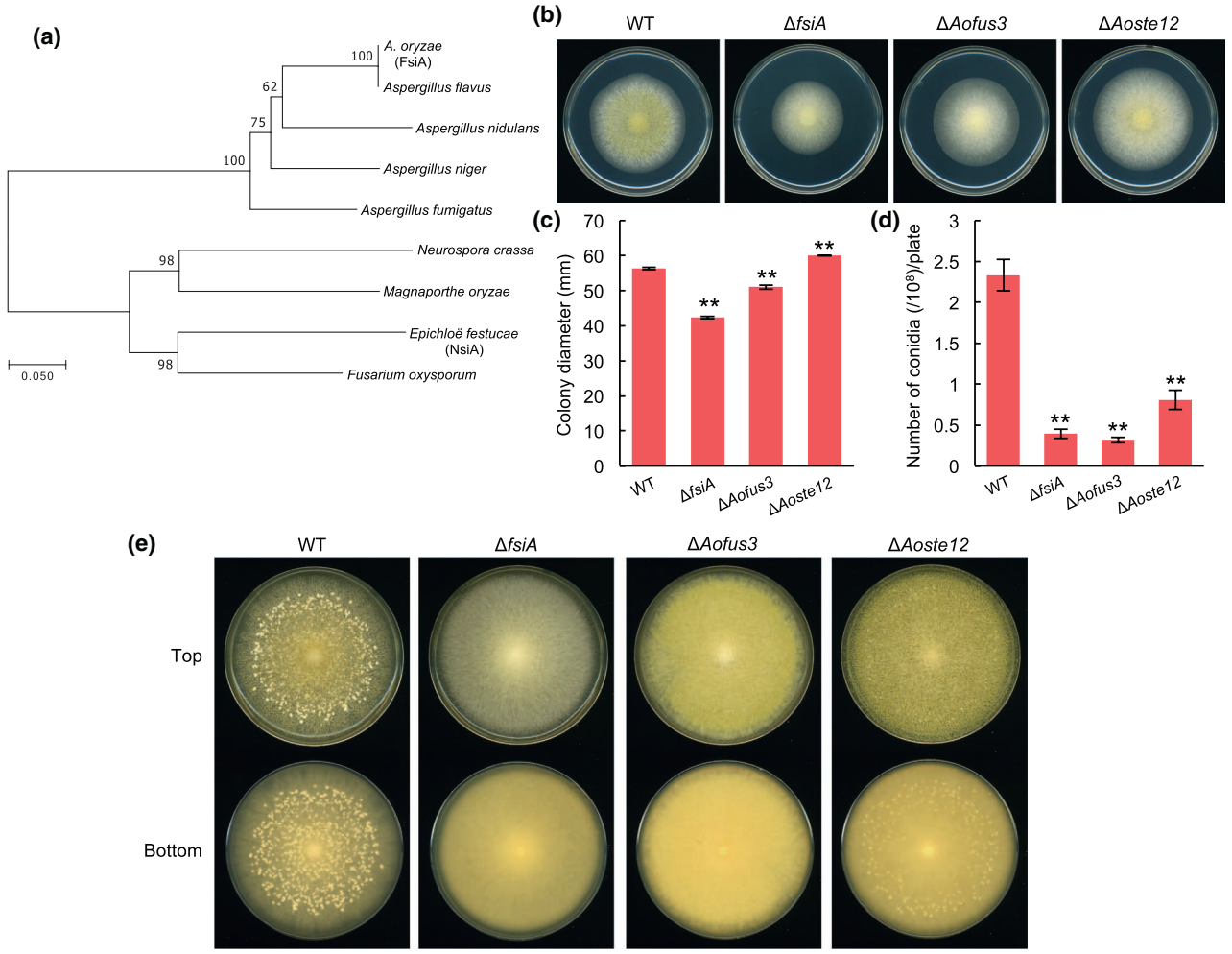

FIGURE 2 Growth, conidiation, and sclerotia formation in the single deletion mutants of *fsiA*, *Aofus3*, and *Aoste12*. (a) Maximum likelihood phylogenetic tree of the FsiA orthologs. (b) Conidial suspension (1×10^4/5 μl) of Ku-1 (WT), ΔfANS-1 (Δ*fsiA*), Δf3NS-1 (Δ*Aofus3*), and Δs12NS-1 (Δ*Aoste12*) was inoculated onto the PD agar medium and incubated in dark at 30°C for 96 hr. (c and d) Growth (c) and conidiation (d) of the strains under the growth condition shown in panel B. Data are shown as means ± *SEM*. of three independent experiments. $^{**}p < .01$ by Student's *t*-test. (e) Conidial suspension (1×10^4/5 μl) of the strains was inoculated onto the ME agar medium and incubated at 30°C for 10 days. Note that sclerotia were observed as white mycelial masses in WT and Δ*Aoste12*

Moreover, all mutants exhibited severe conidiation defects (Figure 2b,d). The deletion mutants of *fsiA* and *Aofus3* did not form any sclerotia, while the *Aoste12* deletion mutant formed fewer sclerotia than the wild-type strain (Figure 2e). These phenotypes were partially or completely suppressed by re-introduction of the deleted genes (Figure S3a–d).

To observe the localization of FsiA, AoFus3 and AoSte12, strains expressing each protein tagged with C-terminal EGFP were constructed. FsiA-EGFP specifically localized to nuclei, and AoSte12-EGFP localized to nuclei and cytoplasm (Figure S4). AoFus3 localized to nuclei and cytoplasm like its ortholog MpkB in *Aspergillus nidulans* (Bayram et al., 2012), and also localized to the center of a septum (Figure S4). The deletion of *fsiA*, *Aofus3*, and *Aoste12* did not affect these localization patterns of the other two proteins (Figure S4). In addition, the effects of their deletion in the interaction between the other two proteins were tested by co-immunoprecipitation. The AoFus3-FsiA, AoFus3-AoSte12, and FsiA-AoSte12 interactions were detected in the deletion mutants of *Aoste12*, *fsiA*, and *Aofus3*, respectively (Figure 1d–f).

2.3 | FsiA, AoFus3, and AoSte12 positively regulate cell fusion-related genes and AonosA

As MAK-2 and PP-1 are essential for cell fusion in *N. crassa* and we also previously showed the requirement of AoFus3 for cell fusion, FsiA is possibly involved in the regulation of cell fusion in *A. oryzae*. Therefore, the cell fusion efficiency of the *fsiA* deletion mutant was quantitatively measured by auxotrophic complementation method, which we previously established (Tsukasaki et al., 2014). In the method, during the mixed culture inoculated with the conidia from two different auxotrophic strains, auxotrophically complemented heterokaryotic conidia are formed as a result of cell fusion. Thus, the ratio of heterokaryotic conidia capable of growing without auxotrophic requirements

represents the cell fusion efficiency. Before the analysis, as the loss of the conidial viability and instability of heterokaryons might artificially show low cell fusion efficiencies, we firstly measured the conidial germination ratios of the heterokaryon generated by protoplast fusion between the two uridine/uracil auxotrophic strains with *pyrG* and *pyrF* gene deletions. As a result, the conidial germination ratios were not different among the wild-type strain and *fsiA*/*Aofus3*/*Aoste12* deletion mutants under both nonselective and selective conditions (Figure S5), indicating that deletions of the three genes do not affect the conidial viability and stability of heterokaryons. We therefore performed the auxotrophic complementation method for analyzing cell fusion efficiency of the deletion mutants. The *fsiA* deletion mutant exhibited a significantly low cell fusion efficiency, while the *Aoste12* deletion mutant showed a moderate defect in cell fusion (Figure 3a) unlike the *pp-1* deletion mutant in *N. crassa* (Herzog et al., 2015). The cell fusion defects were rescued by re-introduction of the deleted genes (Figure S3e).

In order to analyze cell fusion at cellular level, we attempted to develop a method for visualizing fused cells with the Tet-on system, in which expression of the gene of interest is controlled

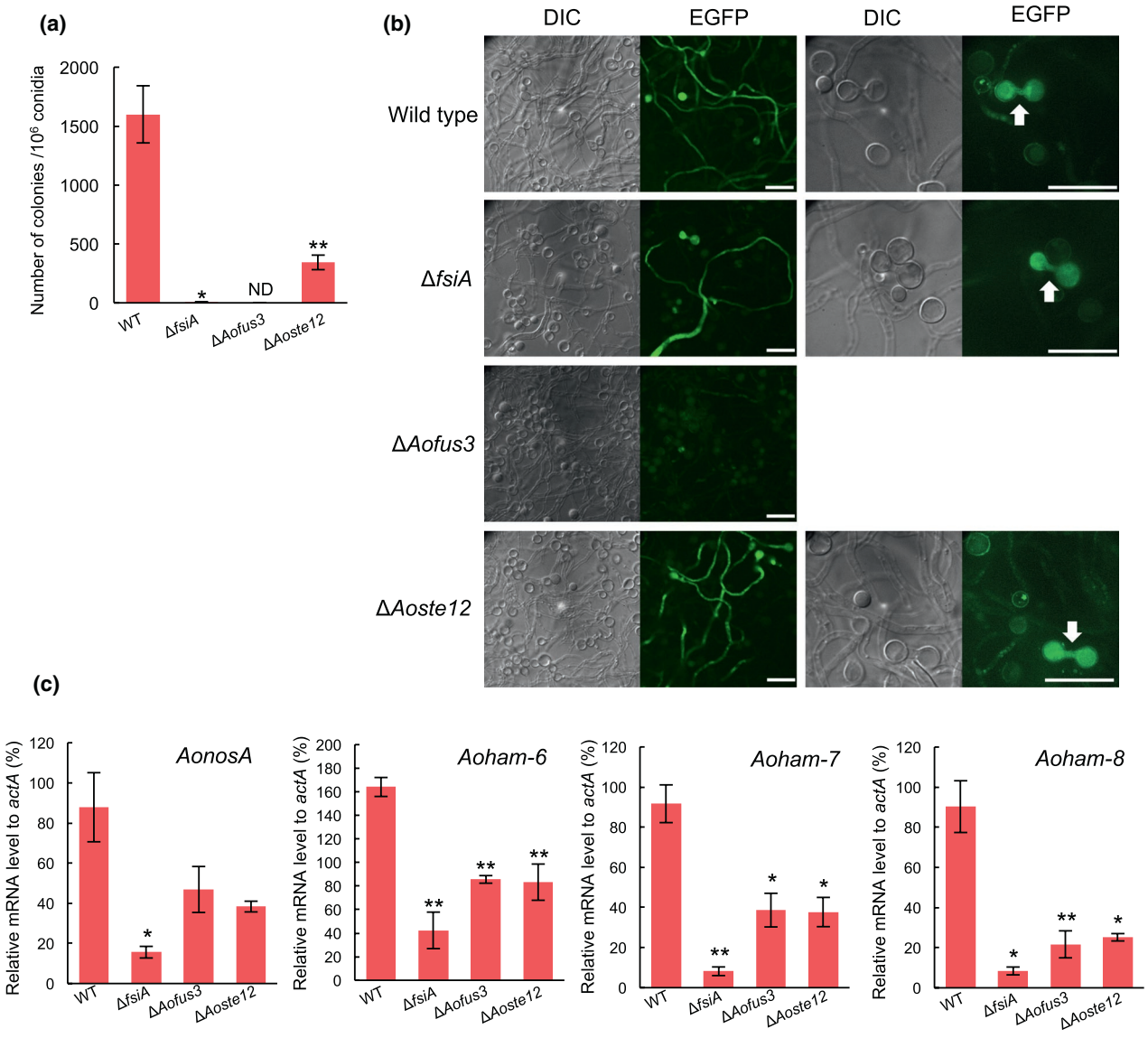

FIGURE 3 Cell fusion efficiency and expression levels of *AonosA*/the cell fusion-related genes in the single deletion mutants of *fsiA*, *Aofus3*, and *Aoste12*. (a) Cell fusion efficiencies between the *pyrG* and *pyrF* deletion strain pairs, KΔpG-1 × KΔpF-1 (WT), ΔfANSΔpG-1 × ΔfANSΔpF-1 (Δ*fsiA*), Δf3NSΔpG-1 × Δf3NSΔpF-1 (Δ*Aofus3*), and Δs12NSΔpG-1 × Δs12NSΔpF-1 (Δ*Aoste12*). (b) Visualization of fused cells in the wild-type strain and *fsiA*/*Aofus3*/*Aoste12* deletion mutants. The conidia of the strains containing the P*tef1-rtTA2*^{s}*-M2* cassette or the *tetO7*::Pmin-*EGFP* cassette were mixed and inoculated onto the CD agar medium containing 0.0015% methionine with 5 μg/ml of doxycycline. After incubation at 30°C for 24 hr, the hyphae were observed by fluorescence microscopy. The white arrows indicate fusion sites. Bars: 20 μm. (c) Conidial suspension (1 × 10^{7}/ml) of Ku-1 (WT), ΔfANS-1 (Δ*fsiA*), Δf3NS-1 (Δ*Aofus3*), and Δs12NS-1 (Δ*Aoste12*) was incubated in 20 ml CD(pH7.0) liquid medium without shaking in dark at 30°C for 48 hr. Total RNA was extracted, and qRT-PCR for the indicated genes was performed. Data are shown as means ± *SEM* of three independent experiments. ND; Not detected, $^{*}p < .05$, and $^{**}p < .01$ by Student's *t*-test

by combining tetracycline-dependent transactivator rtTA2^S-M2 with the rtTA2-M2-dependent *tetO*7::Pmin promoter (Meyer et al., 2011). To investigate its functionality in *A. oryzae*, we constructed a strain expressing rtTA2^S-M2 activator and EGFP under the constitutive *tef1* and tetracycline-responsive *tetO*7::Pmin promoters, respectively. Expectedly, EGFP fluorescence was detected in the presence of a tetracycline derivative, doxycycline (Figure S6a), indicating that the Tet-on system is functional in *A. oryzae*. Subsequently, the rtTA2^S-M2 expression cassette and the EGFP expression cassette under the tetracycline-responsive promoter were separately introduced into individual strains, in which EGFP fluorescence would be detected when cell fusion occurs between the strains (Figure S6b). EGFP fluorescence was detected in the fused cells only when the conidia of these strains were mixed in the presence of doxycycline (Figure S6c). Using the method to visualize fused cells, hyphae with EGFP fluorescence were found in the wild-type strain and *fsiA*/*Aoste12* deletion mutants but not in the *Aofus3* deletion mutant (Figure 3b). The number of hyphae with EGFP fluorescence in the *fsiA* deletion mutant seemed to be lower than those of the wild-type strain and *Aoste12* deletion mutant (Figure 3b). These results indicate that FsiA plays an important role in cell fusion and that the functions of Ste12 ortholog in cell fusion differ between *A. oryzae* and *N. crassa*.

In *N. crassa*, cell fusion-related genes, termed *ham* (Hyphal Anastomosis Mutant), required for cell fusion have been identified (Fu et al., 2011; Jonkers et al., 2016) and are suggested to be regulated by MAK-2 through PP-1 (Leeder et al., 2013). Therefore, FsiA, AoFus3, and AoSte12 could be involved in transcriptional regulation of *ham* gene orthologs (*Aoham-1* - *10* and *14*) in *A. oryzae*. Transcriptional analysis revealed that the mRNA levels of the cell fusion-related genes *Aoham-6*, *Aoham-7*, and *Aoham-8* significantly decreased in all deletion mutants (Figures 3c and S7a). The mRNA level of *Aoham-9* decreased in the *Aofus3* deletion mutant but not the *fsiA* and *Aoste12* deletion mutants, whereas the other *ham* genes were not affected in any deletion mutants (Figure S7a). Recently, PP-1 was shown to stimulate *adv-1* gene encoding another transcription factor for induction of the cell fusion-related genes (Fischer et al., 2018). In addition, the involvement of an *adv-1* ortholog in the expression of *ham* gene orthologs was shown in *A. flavus* (Zhao et al., 2017). The mRNA level of *adv-1* ortholog *AonosA* also significantly decreased in the *fsiA* deletion mutants and showed a tendency to decrease in the *Aofus3* and *Aoste12* deletion mutants (Figure 3c). In the deletion mutants of *AonosA*, *Aoham-6*, *Aoham-7*, and *Aoham-8*, cell fusion was completely abolished (Figure S7b). The downregulation of *AonosA* and the cell fusion-related genes was suppressed by re-introduction of the deleted genes (Figure S7c). These results indicate that FsiA, AoFus3, and AoSte12 regulate cell fusion by controlling *AonosA* and the cell fusion-related genes in *A. oryzae*.

2.4 | FsiA regulates the cell fusion-related genes in an AoSte12-independent manner

To further investigate the transcriptional regulation of *AonosA* and cell fusion-related genes by FsiA, *fsiA*-overexpressing strains were constructed. The *fsiA*-overexpressing strain exhibited a slightly increased growth as compared with the control strain (Figure 4a,b). In the *Aoste12* deletion mutant, this effect was hardly observed when *fsiA* was overexpressed (Figure 4a,b). These results suggest that the increased growth induced by *fsiA* overexpression and by *Aoste12* deletion is redundant. However, *fsiA* overexpression decreased conidiation and sclerotia formation in both the wild-type strain and the *Aoste12* deletion mutant (Figures 4c and S8), indicating that FsiA can negatively regulate conidiation and sclerotia formation in an AoSte12-independent manner. Cell fusion efficiency was significantly decreased by *fsiA* overexpression in the wild-type strain, while this decrease was not observed in the *Aoste12* deletion mutant (Figure 4d), suggesting that AoSte12 contributes to the inhibition of cell fusion by *fsiA* overexpression. In the wild-type strain and the *Aoste12* deletion mutant, *Aoham-6* and *Aoham-8* were induced, and *Aoham-7* showed a tendency to be induced by *fsiA* overexpression, while the cell fusion-related genes except for *ham-7* was not significantly affected in the *Aofus3* deletion mutant (Figure 4e). These results indicate that FsiA can positively regulate the cell fusion-related genes in an AoSte12-independent manner. In contrast, *AonosA* was induced by *fsiA* overexpression in the wild-type strain but not in the *Aofus3* and *Aoste12* deletion mutants (Figure 4e), indicating that FsiA regulates the expression of *AonosA* in a manner dependent on AoFus3 and AoSte12.

2.5 | AoSte12 represses the expression of cell fusion-related genes in the *fsiA* deletion mutant

To clarify the relationship among *fsiA*, *Aofus3*, and *Aoste12*, we investigated their expression levels in each deletion mutant, and observed that each deletion did not affect the expression of the other two genes (Figure S9). Therefore, we next constructed double deletion mutants of these genes.

As the double deletion of *fsiA* and *Aofus3* led to additive defects in growth (Figure 5a,b), suggesting independent functions of FsiA and AoFus3. In contrast, the *Aofus3* and *Aoste12* double deletion mutant exhibited an increased growth as compared with the *Aofus3* deletion mutant (Figure 5a,b). Similarly, the double deletion mutant of *fsiA* and *Aoste12* showed an increased growth as compared with the *fsiA* deletion mutant (Figure 5a,b). These results suggest the involvement of AoSte12 in the growth defects caused by *Aofus3* and *fsiA* deletions.

The conidiation of the single and double deletion mutants of *fsiA* and *Aofus3* was not significantly different (Figure 5c), suggesting their similar functions in conidiation. The *Aofus3* and *Aoste12* double deletion mutant showed a similar conidiation level to that of the *Aofus3* deletion mutant, which was severer than that of the *Aoste12* deletion mutant (Figure 5c). As the conidiation of the *fsiA* and *Aoste12* single and double deletion mutants were almost similar levels (Figure 5c), they possibly have common functions in conidiation. No sclerotia formation were observed in any strains with *Aofus3* deletion (Figure S10), which is probably due to the essential function

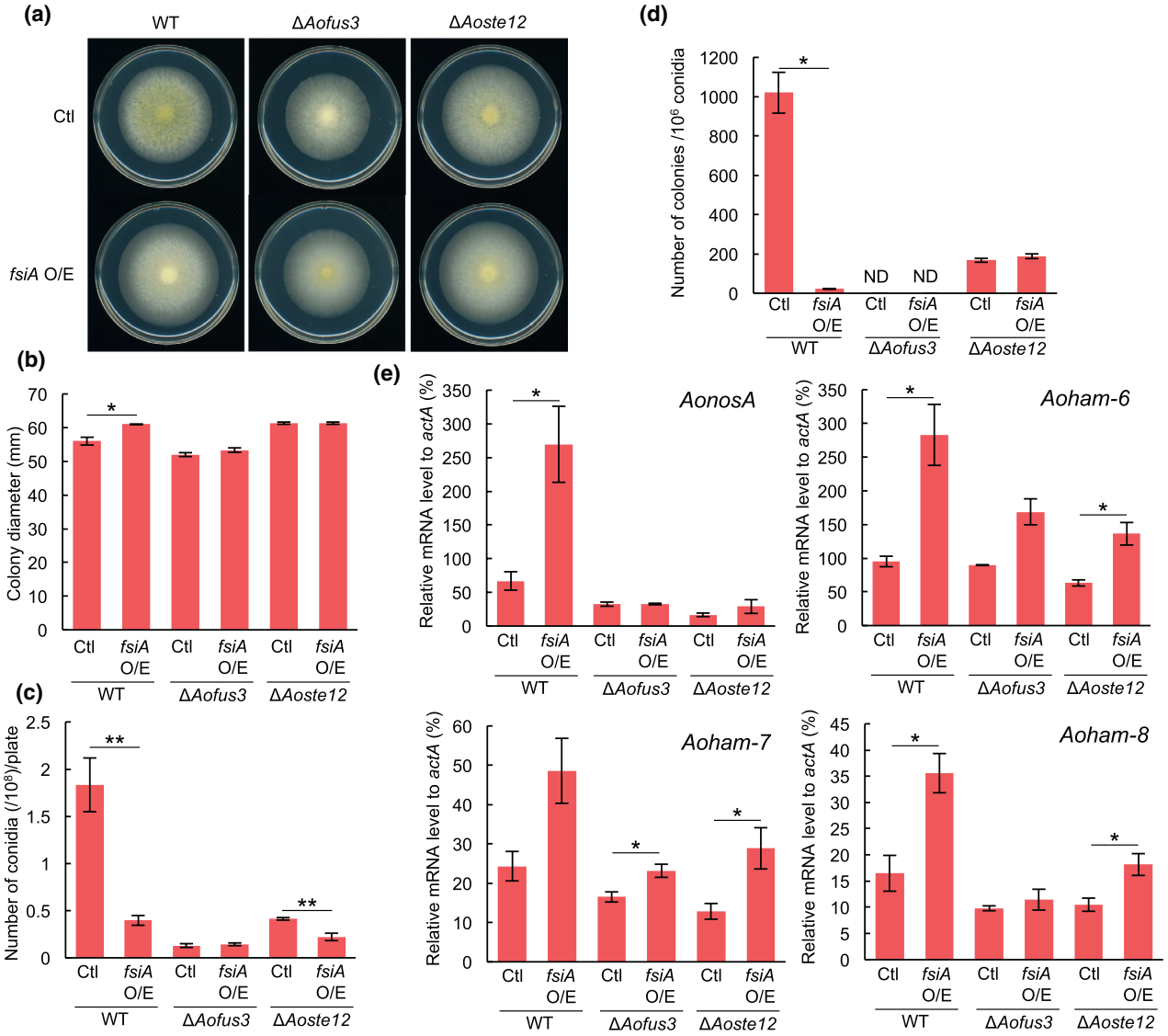

FIGURE 4 Growth, conidiation, cell fusion efficiency, and expression levels of *AonosA*/the cell fusion-related genes in the *fsiA*-overexpressing strains. (a) Conidial suspension (1×10^4/5 μl) of Ku-1 (WT-Ctl), TfANS-1(WT-*fsiA* O/E), Δf3NS-1 (Δ*Aofus3*-Ctl), Δf3TfANS-1 (Δ*Aofus3*-*fsiA* O/E), Δs12NS-1 (Δ*Aoste12*-Ctl), and Δs12TfANS-1 (Δ*Aoste12*-*fsiA* O/E) was inoculated onto the PD agar medium and incubated in dark at 30°C for 96 hr. (b and c) Growth (b) and conidiation (c) of the strains under the growth condition shown in panel A. (d) Cell fusion efficiencies between the *pyrG* and *pyrF* deletion strain pairs, KΔpG-1 × KΔpF-1 (WT-Ctl), TfANSΔpG-1 × TfANSΔpF-1 (WT-*fsiA* O/E), Δf3NSΔpG-1 × Δf3NSΔpF-1 (Δ*Aofus3*-Ctl), Δf3TfANSΔpG-1 × Δf3TfANSΔpF-1 (Δ*Aofus3*-*fsiA* O/E), Δs12NSΔpG-1 × Δs12NSΔpF-1 (Δ*Aoste12*-Ctl), and Δs12TfANSΔpG-1 × Δs12TfANSΔpF-1 (Δ*Aoste12*-*fsiA* O/E). (e) Conidial suspension (1×10^7/ml) of the strains were incubated in 20 ml CD(pH7.0) liquid medium without shaking in dark at 30°C for 48 hr. Total RNA was extracted, and qRT-PCR for the indicated genes was performed. Data are shown as means ± *SEM* of three independent experiments. ND; Not detected, $^*p < .05$, and $^{**}p < .01$ by Student's *t*-test

of AoFus3 in sclerotia formation. Interestingly, the *fsiA* and *Aoste12* double deletion mutant formed sclerotia despite the complete loss of sclerotia formation of the *fsiA* deletion mutant (Figure S10), suggesting that AoSte12 plays a negative role in sclerotia formation in the *fsiA* deletion mutant.

In any strains with *Aofus3* deletion, cell fusion was not detected (Figure 5d), which is can be accounted for by the essential function of AoFus3 in cell fusion as reported previously (Tsukasaki et al., 2014). Among the single and double deletion mutants of *Aofus3* and *fsiA*, the mRNA levels of *AonosA*, *Aoham-7*, and *Aoham-8* were mostly similar (Figure 5e). Similarly, any remarkable difference of their mRNA levels was not detected among the single and double deletion mutants of *Aofus3* and *Aoste12* (Figure 5e). These results suggest the common functions of AoFus3 with FsiA and AoSte12 in the expression of these genes. Surprisingly, the *fsiA* and *Aoste12* double deletion mutant exhibited a higher cell fusion efficiency and increased mRNA levels of *AonosA*, *Aoham-7*, and *Aoham-8* as compared with the *fsiA* single deletion mutant (Figure 5d,e, respectively), suggesting that AoSte12 is capable of negatively affecting the cell fusion ability. In contrast, the *Aoste12* deletion mutant showed a

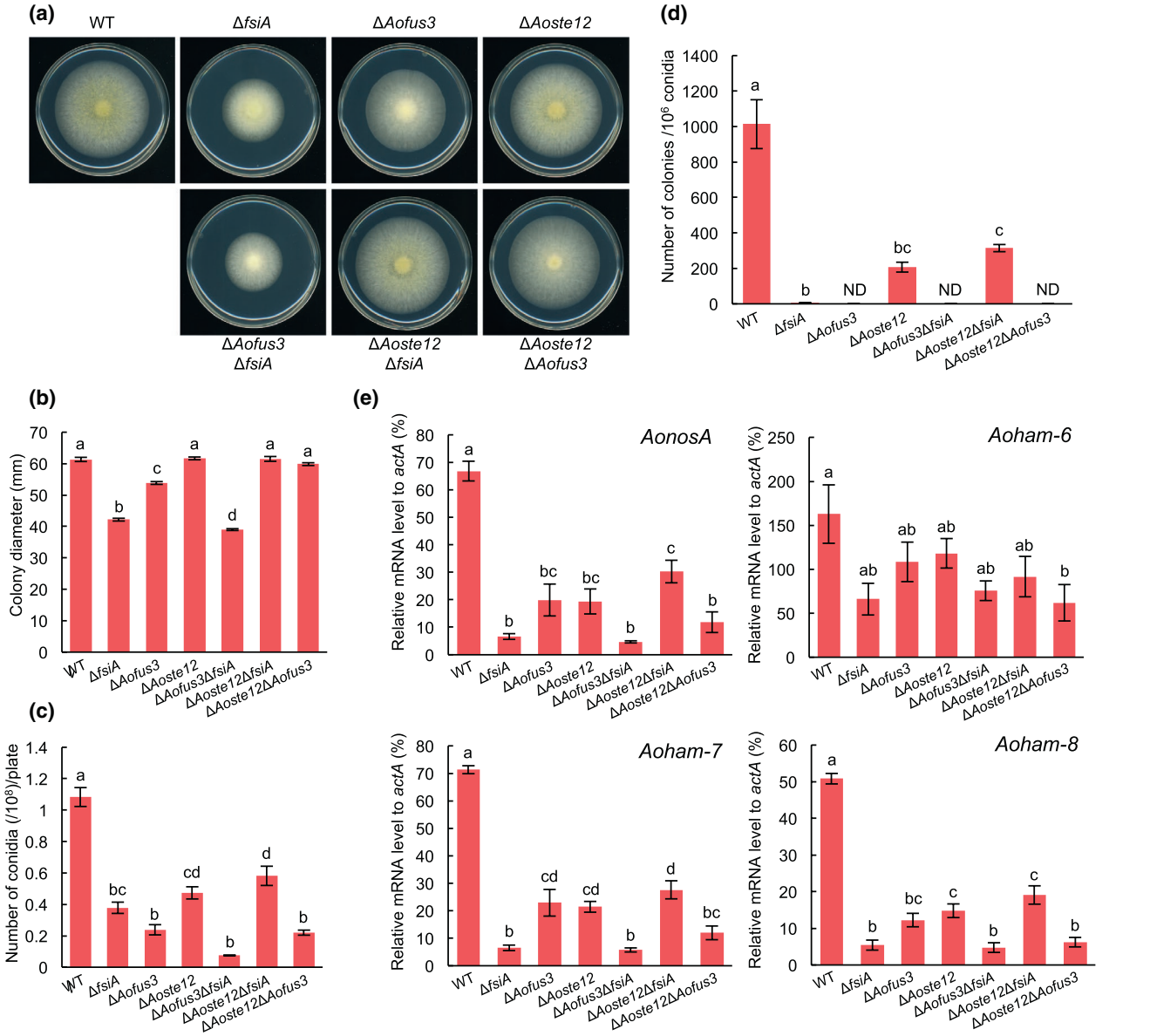

FIGURE 5 Growth, conidiation, cell fusion efficiency, and expression levels of *AonosA*/the cell fusion-related genes in the double deletion mutants of *fsiA*, *Aofus3*, and *Aofus3*. (a) Conidial suspension (1×10^4/5 μl) of Kp-1 (WT), ΔfApNS-1(Δ*fsiA*), Δf3pNS-1 (Δ*Aofus3*), Δs12pNS-1 (Δ*Aoste12*), Δf3ΔfApNS-1 (Δ*Aofus3*Δ*fsiA*), Δs12ΔfApNS-1 (Δ*Aoste12*Δ*fsiA*), and Δs12TΔf3pNS-1 (Δ*Aoste12*Δ*Aofus3*) was inoculated onto the PD agar medium and incubated in dark at 30°C for 96 hr. (b and c) Growth (b) and conidiation (c) of the indicated strains under the growth condition shown in panel A. (d) Cell fusion efficiencies between the *pyrG* and *pyrF* deletion strain pairs, KpΔpG-1 × KpΔpF-1 (WT), ΔfApNSΔpG-1 × ΔfApNSΔpF-1 (Δ*fsiA*), Δf3pNSΔpG-1 × Δf3pNSΔpF-1 (Δ*Aofus3*), Δs12pNSΔpG-1 × Δs12pNSΔpF-1 (Δ*Aoste12*), Δf3ΔfApNSΔpG-1 × Δf3ΔfApNSΔpF-1 (Δ*Aofus3*Δ*fsiA*), Δs12ΔfApNSΔpG-1 × Δs12ΔfApNSΔpF-1 (Δ*Aoste12*Δ*fsiA*), and Δs12Δf3pNSΔpG-1 × Δs12Δf3pNSΔpF-1 (Δ*Aoste12*Δ*Aofus3*). (e) Conidial suspension (1×10^7/ml) of the strains was incubated in 20 ml CD(pH7.0) liquid medium without shaking in dark at 30°C for 48 hr. Total RNA was extracted, and qRT-PCR for the indicated genes was performed. Data are shown as means ± *SEM* of four independent experiments. ND; Not detected. Data are analyzed using Tukey's multiple comparison test, and means sharing the same letter are not significantly different ($p > .05$)

lower cell fusion efficiency and decreased mRNA levels of these genes than the wild-type strain (Figure 5d,e), indicating that the negative function of AoSte12 in cell fusion is recessive as compared with its positive function in the wild-type strain.

To further investigate the function of AoSte12, we constructed *Aoste12*-overexpressing strains, which exhibited severe defects in growth and conidiation (Figure S11a–c) as previously reported by Morita et al. (2007). Moreover, sclerotia formation was delayed by *Aoste12* overexpression in the wild-type strain (Figure S11d). Cell fusion efficiency was significantly decreased by *Aoste12* overexpression in the wild-type strain, and cell fusion ability was completely lost in the *fsiA* deletion mutant (Figure S11e), which indicates the negative function of AoSte12 in cell fusion. However, we could not perform transcriptional analysis of *AonosA* and the cell fusion-related genes in *Aoste12*-overexpressing strains due to their severe growth defects under the tested condition, which hampered mRNA extraction.

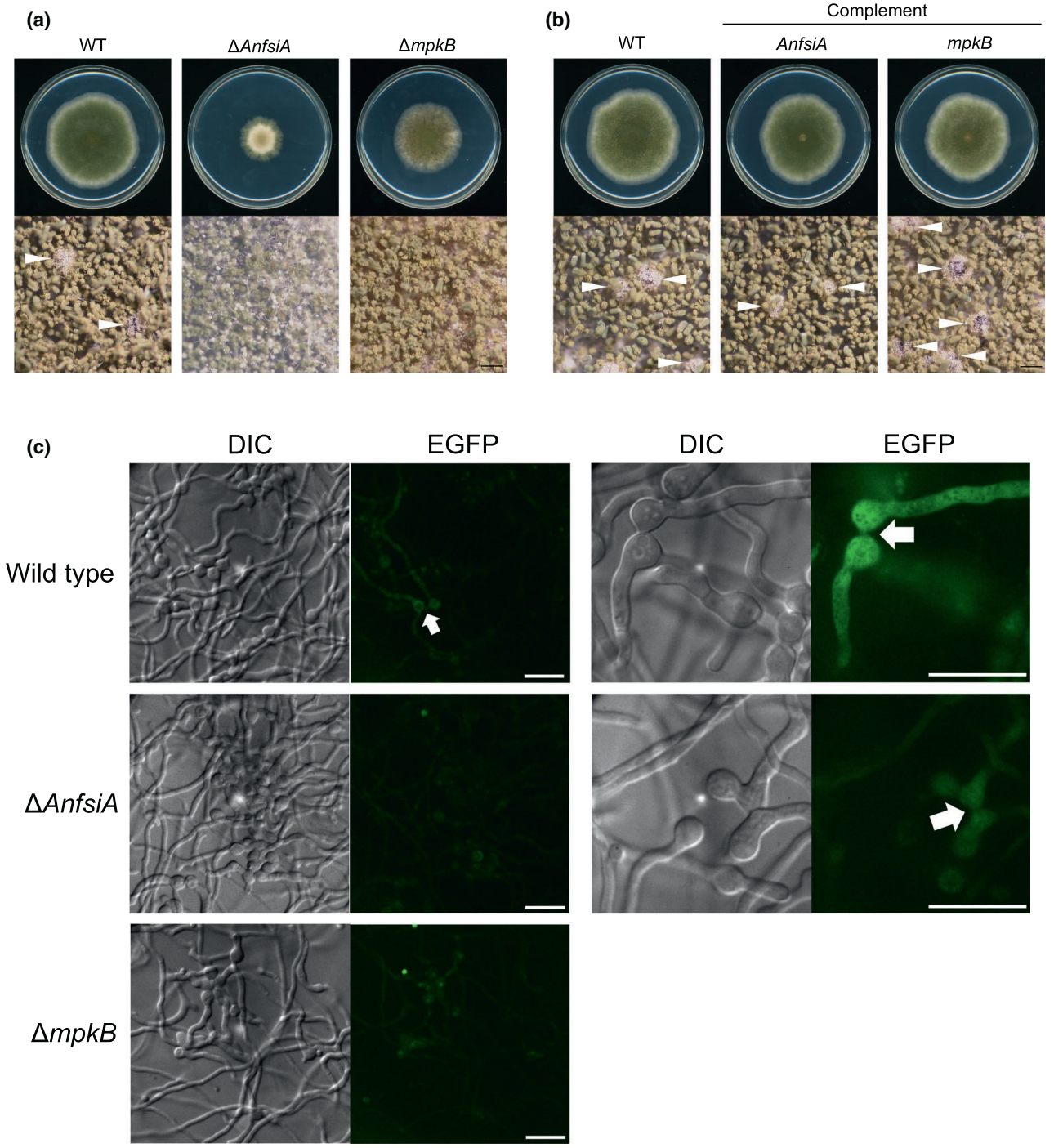

FIGURE 6 Cleistothecia formation of the *AnfsiA* deletion mutant in *A. nidulans*. Conidial suspension (1×10^4/5 μl) of AGB551G (WT), ΔAnfsiA-1 (Δ*AnfsiA*) and ΔmpkB-1 (Δ*mpkB*) (a), and that of AGB551GA (WT), AnfsiA_comp-1 (*AnfsiA* complement) and mpkB_comp-1 (*mpkB* complement) (b) were inoculated onto the GMM agar medium supplemented with uridine, uracil, and pyridoxine, and incubated in dark at 37°C for 120 h. Arrowheads indicate cleistothecia. Bars: 1 mm. (c) Visualization of fused cells in the wild-type strain and *AnfsiA*/*mpkB* deletion mutants. The conidia of the strains containing the P*tef1-rtTA2*^{s}*-M2* cassette and the *tetO7*::Pmin-*EGFP* cassette were mixed and inoculated onto the CD agar medium with 5 μg/ml of doxycycline. After incubation at 30°C for 24 hr, hyphae were observed by fluorescence microscopy. The white arrows indicate fusion sites. Bars: 20 μm

2.6 | The FsiA ortholog is essential for cleistothecia formation in *Aspergillus nidulans*

Sexual developmental structures are formed within sclerotia in *Aspergillus flavus* (Horn et al., 2009), which is genetically close to *A. oryzae* (Gibbons et al., 2012). Furthermore, the Fus3 ortholog MpkB and Ste12 ortholog SteA are essential for sexual development in *A. nidulans*. Therefore, it was predicted that FsiA would also be involved in sexual development due to its role in sclerotia formation (Figure 2e). As sexual reproduction has not been

discovered in *A. oryzae*, we investigated the function of the *fsiA* ortholog termed *AnfsiA* in sexual development in *A. nidulans*. The *AnfsiA* deletion mutant as well as the deletion mutant of *mpkB* did not form any sexual developmental structures such as cleistothecia (Figure 6a). In contrast, the strains re-introduced with the *AnfsiA* gene normally formed cleistothecia (Figure 6b). These results suggest that FsiA is involved in sexual development in *A. nidulans*.

To investigate the function of AnFsiA in cell fusion, we visualized fused cells in *A. nidulans* using the Tet-on system. Fused cells with EGFP fluorescence were easily found in the wild-type stain, but no fused cells were detected in the *mpkB* deletion mutant (Figure 6c). Although fused cells of the *AnfsiA* deletion mutant were hardly found at low magnification, some fused cells were found by detailed observation with high magnification (Figure 6c). This result suggests the low cell fusion efficiency of the *AnfsiA* deletion mutant.

3 | DISCUSSION

In filamentous fungi, whose cell fusion is predicted to be differently regulated from that of yeasts, the function and regulation of Ste12 orthologs have remained unclear. In the present study, we identified the novel protein FsiA as an interactor of AoFus3, which is essential for cell fusion in *A. oryzae* (Tsukasaki et al., 2014). Although the TAP analysis was performed by ectopically expressing AoFus3-TAP with the *AopgkA* promoter, the protein-protein interaction among AoFus3, FsiA, and AoSte12 was also detected by yeast two-hybrid analysis (Figure 1). FsiA is conserved in the filamentous fungal species belonging to Ascomycota (Figure 2a), and the functional involvement of FsiA and AnFsiA, its ortholog of *A. nidulans*, in cell fusion was demonstrated (Figures 3a,b and 6c). NsiA, an FsiA ortholog of the endophytic fungus *Epichloë festucae*, is also involved in cell fusion (Tanaka et al., 2020), indicating that FsiA/NsiA orthologs function in the regulation of cell fusion in filamentous fungi. However, NSI-1, an FsiA/NsiA ortholog of *N. crassa*, is not involved in conidial anastomosis tube fusion (Tanaka et al., 2020). Additionally, Ste12 orthologs are not essential for cell fusion in *A. oryzae*, *E. festucae* and *F. oxysporum* (Figure 3a; Rispail & Di Pietro, 2009; Tanaka et al., 2020) unlike *N. crassa* (Fleißner & Herzog, 2016). These suggest a difference in the regulation mechanism of cell fusion by the FsiA/NsiA and Ste12 orthologs between *N. crassa* and some other filamentous fungi such as *A. oryzae*, *E. festucae*, and *F. oxysporum*.

Fus3 induces the pheromone-responsive genes via the regulation of Ste12 in *S. cerevisiae* (Merlini et al., 2013), and PP-1 is suggested to function downstream of MAK-2 in *N. crassa* (Leeder et al., 2013). The mRNA levels of the cell fusion-related genes *Aoham-6*, *Aoham-7*, and *Aoham-8* decreased in the single and double deletion mutants of *Aofus3* and *Aoste12*, and were almost similar between these deletion mutants (Figures 3c and 5e). These findings suggest that AoSte12 functions downstream of AoFus3 for the regulation of the cell fusion-related genes in *A. oryzae* (Figure 7). Moreover, in *N. crassa*, MAK-2 regulates the expression of *adv-1* encoding another

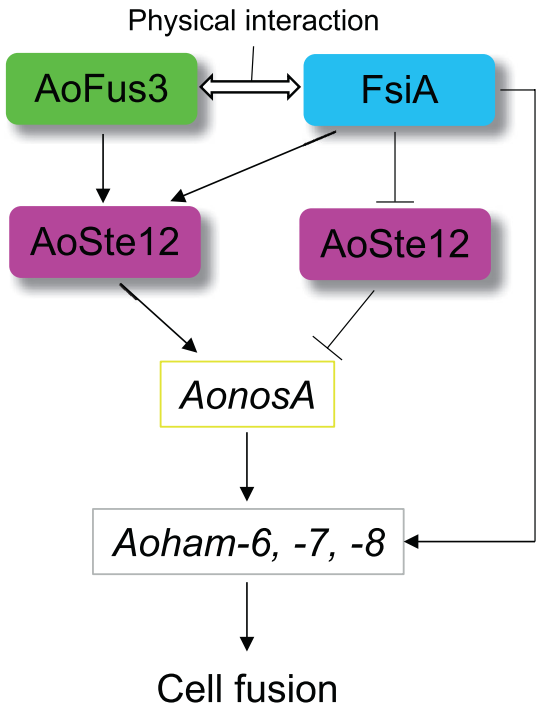

FIGURE 7 Proposed model of the interaction among FsiA, AoFus3, and AoSte12 in the regulation of cell fusion. AoFus3 and AoSte12 positively regulate the *AonosA* expression for induction of the cell fusion-related genes (*Aoham-6*, *-7*, *-8*), in which AoFus3 functions upstream of AoSte12. FsiA is involved in the induction of *AonosA* via AoSte12 and also can induce the cell fusion-related genes independently of AoSte12. AoSte12 regulates the *AonosA* expression not only positively, but also negatively. FsiA suppresses the negative function of AoSte12 in the *AonosA* expression

transcription factor via PP-1 to induce the cell fusion-related genes (Fischer et al., 2018). Since the single deletion mutants of *Aofus3* and *Aoste12* showed decreased mRNA levels of the *adv-1* ortholog *AonosA* as well as of the cell fusion-related genes (Figures 3c and 5e), it is possible that AoFus3 and AoSte12 also control the expression of the cell fusion-related genes via the transcriptional regulation of *AonosA* in *A. oryzae* (Figure 7).

The transcriptional analyses under *fsiA* deletion (Figures 3c and 5e) and *fsiA* overexpression (Figure 4e) indicate that FsiA positively regulates the expression of *AonosA* and the cell fusion-related genes, which is similar to AoFus3 and AoSte12. As *AonosA* induction by *fsiA* overexpression was not detected in the *Aofus3* and *Aoste12* deletion mutants (Figure 4e), FsiA probably can induce the expression of *AonosA* dependently on AoFus3 and AoSte12, leading to induction of the cell fusion-related genes (Figure 7). On the contrary, *fsiA* overexpression induced the expression of the cell fusion-related genes independently of AoSte12 (Figure 4e), suggesting other transcription factor(s) for the FsiA-mediated induction of the cell fusion-related genes (Figure 7). Contrary to the increased expression of the cell fusion-related genes, cell fusion efficiency was decreased by *fsiA* overexpression, which was dependent on AoSte12 (Figure 4d). Considering that *fsiA* overexpression induced the expression of the cell fusion-related genes, not only in the wild-type, but also in

Aoste12 deletion (Figure 4e), the cell fusion-related genes do not seem to cause the decrease of cell fusion efficiency. However, as *AonosA* was induced by *fsiA* overexpression in the wild-type background but not in *Aoste12* deletion, excessive induction of *AonosA* via AoSte12 may inhibit cell fusion.

Importantly, the promotive effects especially in cell fusion and expression of the cell fusion-related genes by *Aoste12* deletion were detected only in *fsiA* deletion (Figure 5d,e). In other words, the negative function of AoSte12 emerged only in the absence of FsiA, indicating that FsiA suppresses the negative function of AoSte12 (Figure 7). Indeed, the negative function of Ste12 was previously suggested in the plant pathogenic filamentous fungus *Colletotrichum lindemuthianum*; an alternative splicing variant of the Ste12 ortholog represses the expression of Ste12-regulated genes when heterologously expressed in the yeast (Wong Sak Hoi et al., 2007). Considering the protein-protein interaction between FsiA and AoSte12 (Figure 1c,f), FsiA does not seem to be involved in splicing of *Aoste12*. In addition, *fsiA* deletion did not affect the protein-protein interaction and localizations of AoFus3 and AoSte12 (Figures 1e and S4). In *S. cerevisiae*, phosphorylation of Ste12 is involved in pheromone response (Wong Sak Hoi & Dumas, 2010), while the key phosphorylation sites identified in Ste12 are not conserved in filamentous fungi (Rispail & Di Pietro, 2010). However, several phosphorylation sites of the Ste12 ortholog PP-1 were identified in *N. crassa* (Jonkers et al., 2014; Xiong et al., 2014), although their physiological significance remains unknown (Fischer et al., 2018). Therefore, FsiA might regulate the phosphorylation of AoSte12, which will be of interest to be investigated in further study.

As the growth defects were observed in the *fsiA* deletion mutant (Figure 2b,c) and the *nsiA* deletion mutants of *E. festucae* (Tanaka et al., 2020), the possibility that the growth defect affected cell fusion efficiency cannot be ignored. However, the protein-protein interaction of FsiA/NsiA with Fus3 and Ste12 orthologs (Figure 1 and Tanaka et al., 2020) substantially supports their functional cooperation in cell fusion. Indeed, *Aofus3* deletion and *Aoste12* overexpression also caused growth defects (Figures 2b,c and S11a,b) similarly to the previous reports in other filamentous fungi (Jun et al., 2011; Ma et al., 2016; Morita et al., 2007; Priegnitz et al., 2015; Rispail & Di Pietro, 2009; Vallim et al., 2000), indicating the involvement of Fus3 and Ste12 orthologs in growth. Interestingly, the growth defects by *fsiA* and *Aofus3* deletions were dependent on AoSte12 (Figure 5a,b), indicating the negative function of AoSte12 in the growth regulation by FsiA and AoFus3. These phenomena are in contrast to the increased mRNA levels by the *Aoste12* deletion in the deletion mutant of *fsiA* but not *Aofus3* (Figure 5e), suggesting a differential regulation of growth and cell fusion by AoSte12.

The defects of sclerotia formation and cell fusion were coincidentally observed in the single deletion mutants (Figures 2e and 3a) and the *fsiA*- and *Aoste12*-overexpressing strains (Figures 4d, S8, and S11D), and both defects of the *fsiA* deletion mutant were recovered by *Aoste12* deletion (Figures 5d and S10). In *A. flavus*, the orthologs of the cell fusion-related genes are essential for sclerotia formation (Zhao et al., 2017). Therefore, it is suggested that FsiA, AoFus3, and AoSte12 regulate sclerotia formation via the cell fusion-related genes. Moreover, the FsiA ortholog *AnfsiA* is involved in cleistothecia formation along with MpkB (Figure 6) (Paoletti et al., 2007) and SteA (Vallim et al., 2000), demonstrating an important role of FsiA in sexual development. In *A. flavus*, the sexual developmental structures are formed within sclerotia (Dyer & O'Gorman, 2012; Horn et al., 2009), and genes involved in sexual development are also related to sclerotia formation (Cary et al., 2012; Zhao et al., 2017), which suggests a common regulatory mechanism for these two development processes. In addition, the genes involved in cell fusion are related to sexual development in *N. crassa* (Fischer et al., 2018). Thus, it is proposed that FsiA is involved in sexual development by regulating the cell fusion-related genes in filamentous fungi.

In the present study, we identified the novel cell fusion-regulator FsiA and showed its AoSte12-dependent and -independent functions in the regulation of cell fusion-related genes in *A. oryzae*. Importantly, the AoSte12-independent function indicates the existence of an unrevealed regulatory mechanism of cell fusion in filamentous fungi. Although the functional relationship between FsiA and AoFus3 remains controversial, their physical interaction found in this study would reflect a specialized regulation mechanism for cell fusion. Further investigation into the molecular machinery originated from the three proteins will provide clues for the cell fusion ability specifically evolved in Ascomycete filamentous fungi but not present in yeasts.

4 | EXPERIMENTAL PROCEDURES

4.1 | Strains and culture conditions

The *A. oryzae*, *A. nidulans*, and *S. cerevisiae* strains used in this study are listed in Supplementary Table S1. Czapek-dox (CD) medium (CD(Glc): 3 g/L $NaNO_3$, 2 g/L KCl, 1 g/L KH_2PO_4, 0.5 g/L $MgSO_4.7H_2O$, 0.002 g/L $FeSO_4.7H_2O$, and 20 g/L glucose) and potato dextrose (PD) medium (Nissui, Tokyo, Japan) were used for the growth of *A. oryzae*. DPY medium (2% dextrin, 1% hipolypeptone (Wako, Osaka, Japan), 0.5% yeast extract, 0.5% KH_2PO_4, and 0.05% $MgSO_4.7H_2O$) was used for the TAP analysis. Malt extract (ME) medium (2% malt extract, 2% glucose, and 0.1% hipolypeptone) was used to induce sclerotia formation of *A. oryzae*. For selection using the *ptrA* marker, 100 ng/μl pyrithiamine was added. For the growth of *sC* mutants, 0.0015% methionine was added into the CD medium. CD medium containing 20 g/L dextrin instead of glucose (CD(Dex)) was used for strong induction of the *amyB* promoter. GMM medium (0.52 g/L KCl, 0.52 g/L $MgSO_4.7H_2O$, 1.52 g/L KH_2PO_4, 0.85 g/L $NaNO_3$, 10 g/L glucose, and 0.1% Trace element solution (Rowlands & Turner, 1973)) was used for the growth of *A. nidulans*. For the growth of *pyrG/AnpyrG* and *pyrF* mutants, 5 g/L uridine and 2 g/L uracil were added. For the growth of *pyroA* mutants, 0.5 mg/L pyridoxine was added. CD medium adjusted pH 7.0 (CD(pH7.0)) was also used to induce cell fusion. The SD medium for the growth of *S. cerevisiae* was prepared as described in Yeast Protocols Handbook (Clontech Laboratories, Mountain View, CA, USA).

4.2 | DNA manipulation and transformation of *A. oryzae* and *A. nidulans*

Escherichia coli DH5α was used for DNA manipulation. The polymerase chain reaction (PCR) was performed using PrimesSTAR HS DNA polymerase (TaKaRa, Otsu, Japan). The In-Fusion® HD Cloning Kit (Clontech Laboratories), the Zero Blunt® TOPO® PCR cloning kit for sequencing (Thermo Fisher Scientific, Waltham, MA, USA), and the MultiSite Gateway™ system (Thermo Fisher Scientific) were used for plasmid construction. Primers used in this study are listed in Supplementary Table S2. Transformation of *A. oryzae* and *A. nidulans* was performed as described previously (Ichinomiya et al., 2002; Maruyama & Kitamoto, 2011).

4.3 | Construction of the strains for the TAP analysis of AoFus3

The plasmid for the expression of AoFus3 tagged with TAP tag at its C-terminus was constructed by the MultiSite Gateway™ system. The plasmid pg5′Pp containing the *AopgkA* promoter (Mabashi et al., 2006) was used as a 5′ entry clone. The *Aofus3* ORF was amplified from the genomic DNA of the *A. oryzae* strain RIB40 using the primers attB4-Aofus3-F/attB1-Aofus3-R, and cloned into pDONR™221 vector by the BP recombination reaction, yielding the center entry clone. The TAP tag was amplified from pME3156 (Bayram et al., 2008) using the primers aB2-CTAP-F/aB3-CTAP-R, and cloned into pDONR™P2R-P3 by the BP recombination reaction, yielding the 3′ entry clone. The inserted sequences of these entry clones were assembled with the destination vector pgDN (Mabashi et al., 2006) by the LP recombination reaction, yielding pgPF3TN for expression of AoFus3-TAP under the *AopgkA* promoter. This plasmid was introduced into the strain NSRKu70-1-1A (Escaño et al., 2009), yielding the strain SK-F3T.

4.4 | Construction of the single and double deletion mutants of *fsiA*, *Aofus3*, and *Aoste12*

The plasmid pΔfsiA for the replacement of *fsiA* with *adeA* was constructed as follows: the 5′ and 3′-flanking regions of *fsiA* and the *adeA* fragment were amplified from the genomic DNA of RIB40 using the primer sets, 19IF-fsiA-5F/adeA-fsiA-5R, adeA-fsiA-3F/19IF-fsiA-3R, and adeA-F/R, respectively. These three fragments were fused using the primers 19IF-fsiA-5F/19IF-fsiA-3R and ligated with the *Bam*HI-digested pUC19 by In-Fusion reaction, yielding the plasmid pΔfsiA. The DNA fragment amplified from pΔfsiA using the primers 19IF-fsiA-5F/19IF-fsiA-3R was introduced into the strain NSRKu70-1-1 (Escaño et al., 2009), yielding the strain ΔfsiA-1 (Figure S12a).

The plasmid pΔs12 for the replacement of *Aoste12* with *adeA* was constructed as follows: the 5′ and 3′-flanking regions of *Aoste12* were amplified from the genomic DNA of RIB40 using the primer sets, ste12-5UTR-F/ste12-5UTR-adeA-R and adeA-ste12-3UTR-F/ste12-3UTR-R, respectively. The *adeA* fragment was amplified from pgEaA (Jin et al., 2007) using the primers ste12-5UTR-adeA-F/adeA-ste12-3UTR-R. These three fragments were fused using the primers ste12-5UTR-F/ste12-5UTR-R and ligated with pCR®4Blunt-TOPO, yielding the plasmid pΔs12. The DNA fragment amplified from pΔs12 using the primers ste12-5UTR-F/ste12-5UTR-R was introduced into the strain NSRKu70-1-1, yielding the strain NSK-Δs12-1 (Figure S12b).

The plasmid pΔfsiAptrA for the replacement of *fsiA* with *ptrA* was constructed as follows: the 5′ and 3′-flanking regions of *fsiA* were amplified from the genomic DNA of RIB40 using the primer sets, 19IF-fsiA-5F/ptrA-fsiA-5R and ptrA-fsiA-3F/19IF-fsiA-3R, respectively. The *ptrA* fragment was amplified from the plasmid pPTRII (TaKaRa) using the primers ptrAF/R. These three fragments were fused using the primers 19IF-fsiA-5F/19IF-fsiA-3R and ligated with the *Bam*HI-digested pUC19 by In-Fusion reaction, yielding the plasmid pΔfsiAptrA. The DNA fragment amplified from pΔfsiAptrA using the primers 19IF-fsiA-5F/19IF-fsiA-3R was introduced into the strains NSK-Δf3 and NSK-Δs12-1, yielding the strains Δfus3ΔfsiAp-1 and Δste12ΔfsiAp-1, respectively (Figure S12c).

The plasmid pΔfus3ptrA for the replacement of *Aofus3* with *ptrA* was constructed as follows: the 5′ and 3′-flanking regions of *Aofus3* were amplified from the genomic DNA of RIB40 using the primer sets, 19IF-fus35F/ptrA-fus3_5R and ptrA-fus3_3F/19IF-fus33R, respectively. The *ptrA* fragment was amplified from pPTRII using the primers ptrAF/R. These three fragments were fused using the primers 19IF-fus35F/19IF-fus33R and ligated with the *Bam*HI-digested pUC19 by In-Fusion reaction, yielding the plasmid pΔfus3ptrA. The DNA fragment amplified from pΔfus3ptrA using the primers 19IF-fus35F/19IF-fus33R was introduced into the strain Δs12N-1, yielding the strain Δs12Δf3pN-1 (Figure S12d).

4.5 | Construction of the strains overexpressing *fsiA* and *Aoste12*

The plasmid pUXNTfA for *fsiA* overexpression was constructed as follows; the *Aotef1* promoter and terminator were amplified from the genomic DNA of RIB40 using the primer sets, UTX-Ptef1F/Ptef1R, and Ptef1-Ttef1F/UTX-Ttef1R, respectively. These fragments were fused using the primers UTX-Ptef1F/UTX-Ttef1R and ligated with the *Xho*I-digested pUXN (Mori et al., 2019) by In-Fusion reaction, yielding the plasmid pUXNtef1, which contains the *Sma*I site between the *Aotef1* promoter and terminator. The *fsiA* ORF amplified from the genomic DNA of RIB40 using the primers tef1-fsiAF/R was ligated with the *Sma*I-digested pUXNtef1 by In-Fusion reaction, yielding the plasmid pUXNTfA. The *Not*I-digested pUXNTfA was introduced into the *A. oryzae niaD*$^{-}$ strains (Figure S12e).

The plasmid pUtAs12 for *Aoste12* overexpression was constructed as follows; the *Aoste12* ORF amplified from the genomic DNA of RIB40 using the primers PamyB-ste12F/TamyB-ste12R was ligated with the *Sma*I-digested pUtNAN (Katayama et al., 2019) by In-Fusion reaction, yielding the plasmid pUtAs12, which

contains *Aoste12* downstream of the *amyB* promoter. The *Not*I-digested pUtAs12 was introduced into the *A. oryzae niaD*$^{-}$ strains (Figure S12f).

4.6 | Construction of the deletion mutants of *AnfsiA* and *mpkB* in *A. nidulans*

The plasmids pΔAnfsiA and pΔmpkB for the replacement of *AnfsiA* and *mpkB* with *AnpyrG*, respectively, were constructed as follows; the 5′ and 3′-flanking regions of these genes and the *AnpyrG* fragment were amplified from the genomic DNA of *A. nidulans* wild-type strain FGSC A4 using the primer sets, 19IF-AnfsiA5F/pG-AnfsiA5R, pG-AnfsiA3F/19IF-AnfsiA3R, 19IF-mpkB5F/pG-mpkB5R, pG-mpkB3F/19IF-mpkB3R, and AnpyrGF/R, respectively. The 5′ and 3′-flanking regions and the *AnpyrG* fragment were ligated with the *Bam*HI-digested pUC19 by In-Fusion reaction, yielding the plasmids pΔAnfsiA and pΔmpkB. The DNA fragments amplified from pΔAnfsiA and pΔmpkB using the primer sets, 19IF-AnfsiA5F/19IF-AnfsiA3R and 19IF-mpkB5F/19IF-mpkB3R were introduced into the AGB551 strain, yielding the strains ΔAnfsiA-1 and ΔmpkB-1, respectively (Figure S12g,h).

4.7 | Construction of strains for detection of fused cells using the Tet-on system

The plasmid pUXNT-Ton-EGFP to investigate the functionality of Tet-on system in *A. oryzae* was constructed as follows; the DNA fragment containing the transactivator gene *rtTA2*^{S}*-M2* and *Aspergillus fumigatus cgrA* terminator (T*cgrA*) was amplified from the plasmid pVG2.2 (Meyer et al., 2011) using the primers tefIF-rtTA2s-M2-F/TAfcgrAR. The DNA fragment containing seven copies of the tetracycline responsive element (*tetO7*) and the minimal promoter sequence of *A. nidulans gpdA* promoter (Pmin) was amplified from pVG2.2 using the primers TcgrA-tetO7F/Pmin-R. The EGFP encoding gene was amplified from pUt-C-EGFP (Mori et al., 2019) using the primers Pmin-ClinkerF/Ttef-CEGFPR. The three fragments were ligated with the *Sma*I-digested pUXNtef1 by In-Fusion reaction, yielding pUXNT-Ton-EGFP, in which *rtTA2*^{S}*-M2* locates at the downstream of the *tef1* promoter, and *EGFP* locates at the downstream of the tetracycline-responsive *tetO7*::Pmin promoter.

The plasmids pUXN-TonA and pUXN-TonBG for detecting fused cells in *A. oryzae* were constructed as follows; the P*Aotef1-rtTA2*^{S}*-M2*-T*cgrA* fragment was amplified from pUXNT-Ton-EGFP using the primers UTX-Ptef1F/XNIF-TAfcgrAR, and then ligated with the *Xho*I-digested pUXN by In-Fusion reaction, yielding the plasmid pUXN-TonA. The *tetO7*::Pmin-EGFP-T*tef1* fragment was amplified from pUXNT-Ton-EGFP using the primers XNIF-tetO7-F/ UTX-Ttef1R, and then ligated with the *Xho*I-digested pUXN by In-Fusion reaction, yielding the plasmid pUXN-TonBG.

The plasmids pAnwADN-TonA and pAnwADN-TonBG for detecting fused cells in *A. nidulans* were constructed as follows; the upstream and middle regions of *A. nidulans wA* gene and *pyroA* marker were amplified from the genomic DNA of FGSC A4 using the primer sets, AnwA-1/-2, AnwA-3/-4, and pyroAF/R, respectively. These fragments were ligated with the *Bam*HI-digested pUC19 by In-Fusion reaction, yielding the plasmid pAnwADN. The *tef1* promoter of *A. nidulans* amplified from the genomic DNA of FGSC A4 using the primers wAIF-PAntef1F/wAIF-rtTA2s-PAntef1R and *rtTA2*^{S}*-M2-*T*cgrA* fragment amplified from pUXN-TonA using the primers wAIF-rtTA2s-M2F/wAIF-TAfcgrAR were ligated with the *Hpa*I-digested pAnwADN by In-Fusion reaction, yielding the plasmid pAnwADN-TonA. The *tetO7*::Pmin-*EGFP-TAotef1* fragment was amplified from pUXN-TonBG using the primers wAIF-tetO7F/wAIF-TAotef1R, and then ligated with the *Hpa*I-digested pAnwADN by In-Fusion reaction, yielding the plasmid pAnwADN-TonBG.

4.8 | Tandem affinity purification (TAP) analysis

TAP analysis was performed as previously described with some modifications (Bayram et al., 2008). The strain SK-F3T was incubated at 30°C for 1 day in the DPY liquid medium, in which the expression of AoFus3-TAP fusion protein was induced. The collected mycelia were homogenized in liquid nitrogen with mortar and pestle. The homogenized mycelia were suspended with the B250 buffer (250 mM NaCl, 1% glycerol, 0.1% NP-40, 1 mM EDTA, 10 mM Tris-HCl (pH 7.5)), and mycelial debris was removed by centrifugation at 20,000*g* for 30 min at 4°C. The supernatant was incubated with the IgG sepharose, washed with the B250 buffer, on a rotating platform at 4°C for 3 hr. The IgG sepharose was collected using chromatography columns and washed twice with the W250 buffer (250 mM NaCl, 0.1% NP-40, and 4 mM Tris-HCl (pH 8.0)), once with the W150 buffer (150 mM NaCl, 0.1% NP-40, and 4 mM Tris-HCl (pH 8.0)) and once with TEV cleavage buffer (TCB: 150 mM NaCl, 0.1% NP-40, 1 mM DTT, 0.25 mM EDTA, and 4 mM Tris-HCl (pH 8.0)). Then, the IgG sepharose was suspended with the TCB containing AcTEV™ enzyme (Promega, Madison, WI, USA) and incubated on a rotating platform at 4°C overnight. The supernatant was added into the calmodulin binding buffer (CB buffer: 150 mM NaCl, 1 mM magnesium acetate, 2 mM $CaCl_2$, 1 mM imidazole, 0.07% 2-mercaptoethanol, 4 mM Tris-HCl (pH 8.0)) containing the calmodulin affinity resin washed with the CB buffer in the new columns and rotated at 4°C for 1 hr. After incubation, the resin was washed three times with the CB buffer containing 0.02% NP-40. Then, proteins retained on the resin were eluted twice by adding the elution buffer (120 mM NaCl, 0.07% NP-40, 1 mM magnesium acetate, 1 mM imidazole, 0.07% 2-mercaptoethanol, 20 mM EGTA, 4 mM Tris-HCl (pH 8.0). The eluted samples were concentrated by the TCA precipitation and prepared as the protein samples for SDS-PAGE. After separation of the protein samples by SDS-PAGE and staining with Coomassie Brilliant Blue G, each lane of the SDS-PAGE gel was cut into eight pieces.

Tryptic in-gel digestion was performed according to Shevchenko et al. (2006) with sequencing grade trypsin (Promega). Tryptic

peptides were analyzed on an UltiMate 3000 nano-HPLC system (Dionex, Sunnyvale, CA, USA) operated with Xcalibur (Thermo Finnegan, San Jose, CA, USA) through DCMS Link (Dionex) with μ-Precolumn™ cartridge Acclaim PepMap100 C18, 5 μm, 100 Å, 300 μm inner diameter, 5 mm (Dionex P/N 160454), analytical capillary column; 75 μm inner diameter, 15 cm, Acclaim PepMap100 C18, 3 μm (Dionex P/N 160321), ion trap mass spectrometer (LCQ DecaXPplus, Thermo Scientific), and a PicoTip™ emitter FS360-20-10 (New Objective, Woburn, MA, USA). For LC/MS, typically 10 μl sample was loaded on a μ-Precolumn™ cartridge and washed for 8 min at a flow rate of 30 μl/min. The gradient nano-flow (200 nl/min) transferred the peptides to the analytical capillary column. A solvent gradient from 5% B (84% acetonitrile, 16% water, 0.07% formic acid) to 50% B within 40 min was applied. Columns were cleansed with 95% B followed by pre-equilibration (5% B). Peptides eluting during the 40-min gradient were online transferred to MS by electrospray ionization (ESI) through the use of a PicoTip™ emitter and a spray voltage of 1.5 kV. During the LC gradient, the mass spectrometer cycled through the acquisition of a full MS scan within the mass range of 300 to 1,400 Da followed by four data-dependent, collision-induced, MS/MS spectra of the four most intense ions. The dynamic exclusion was set at exclusion mass width 3 Da, repeat count 2, repeat duration 0.5 min, exclusion list size 50, and exclusion duration 1 min. Spectra were collected in centroid mode. MS/MS spectra were analyzed with the TurboSEQUEST (Bioworks Browser 3.3.1 package; Thermo Finnigan) using the *A. oryzae* protein sequences in the *Aspergillus* Genome database (AspGD; http://www.aspgd.org). Search parameters for TurboSEQUEST were: (i) precursor ion mass tolerance less than 1.4 atomic mass units, (ii) fragment ion mass tolerance less than 1.0 atomic mass unit, (iii) up to three missed tryptic cleavages allowed, and (iv) fixed cysteine modification by carboxyamidomethylation (plus 57.05 atomic mass units) and variable modification by methionine oxidation (plus 15.99 atomic mass units). Matching peptides for protein identification had to pass the following filters: (i) cross-correlation scores (Xcorr) over 2.5, (ii) *p* value below 5.0E-02, and (iii) primary scores (Sp) of at least 500.

4.9 | Construction of other plasmids and strains

Construction of the other plasmids and strains is described in Supporting Information.

4.10 | Measurement of cell fusion ability

Quantitative analysis of cell fusion was performed as described previously (Tsukasaki et al., 2014). The conidia of the *pyrG* deletion mutants and the *pyrF* deletion mutants were mixed and inoculated onto the CD agar medium containing uridine and uracil. After 5-days incubation, formed conidia were spread on the CD agar medium containing 0.1% Triton-X 100 and incubated for 2 days. Then, the number of colonies were counted.

4.11 | Visualization of fused cells using Tet-on system

Conidial suspension (10^7/ml) of the strain expressing *rtTA2^S-M2* was mixed with the equal volume of conidial suspension (10^7/ml) of the strain, in which the *EGFP* gene was expressed under the *tetO7*::Pmin promoter. The 10 μl aliquots of the mixed suspension were spotted onto the CD agar medium containing 0.0015% methionine with and without 5 μg/ml of doxycycline, and incubated at 30°C. After 16 hr, a piece of agar medium was cut, and hyphae were observed by fluorescence microscopy.

4.12 | Extraction of total RNA and real time RT-PCR

Total RNA was extracted from mycelia homogenized with a multi-beads shocker (Yasui Kikai, Osaka, Japan) using Isogen (NIPPON GENE, Tokyo, Japan). The cDNA was synthesized from the isolated RNA by reverse transcription using PrimeScript RT reagent Kit with gDNA Eraser (Perfect Real Time) (TaKaRa). The mRNA level was analyzed using TB Green™ *Premix Ex Taq*™ II (Tli RNaseH Plus) (TaKaRa) and Thermal Cycler Dice Real Time System (TaKaRa). The primer sequences are listed in Supplementary Table S2.

4.13 | RACE analysis

RACE analysis was performed as described previously (Mori et al., 2019). The primer set, fsiA-GSP-F/fsiA-GSP-Fnest/fsiA-GSP-R/fsiA-GSP-Rnest, was used as gene-specific primers to *fsiA* (AO090701000086).

ACKNOWLEDGMENT

This study was financially supported by Japan Society for the Promotion of Science (JSPS) KAKENHI Grant Number JP17K15242, Grant-in-Aid for Young Scientists (B), and 18H02123, Grant-in-Aid for Scientific Research (B), and Science Foundation Ireland 13/CDA/2142 to Ö. B.

CONFLICT OF INTEREST

The authors declare that they have no conflict of interest with the contents of this article.

AUTHOR CONTRIBUTIONS

TK: conception and design: acquisition, analysis, and interpretation of the data; writing. ÖB: acquisition, analysis, and interpretation of the data. TM: acquisition, analysis, and interpretation of the data. BK: acquisition and analysis of the data. OV: acquisition, analysis, and interpretation of the data. DT: conception and design: interpretation of the data. GB: conception and design: interpretation of the data. KK: conception and design: interpretation of the data. JM: conception and design: acquisition, analysis, and interpretation of the data; writing.

ORCID

Özgür Bayram https://orcid.org/0000-0002-0283-5322
Betim Karahoda https://orcid.org/0000-0001-8667-7378
Daigo Takemoto https://orcid.org/0000-0002-9816-7882
Gerhard H. Braus https://orcid.org/0000-0002-3117-5626
Jun-ichi Maruyama https://orcid.org/0000-0002-5318-5366

REFERENCES

Bayram, Ö., Bayram, Ö.S., Ahmed, Y.L., Maruyama, J., Valerius, O., et al. (2012) The *Aspergillus nidulans* MAPK module AnSte11-Ste50-Ste7-Fus3 controls development and secondary metabolism. *PLoS Genetics*, *8*, e10002816.

Bayram, Ö., Krappmann, S., Ni, M., Bok, J.W., Helmstaedt, K., et al (2008) VelB/VeA/LaeA complex coordinates light signal with fungal development and secondary metabolism. *Science*, *320*, 1504–1506.

Cary, J.W., Harris-Coward, P.Y., Ehrlich, K.C., Mack, B.M., Kale, S.P., Larey, C., et al. (2012) NsdC and NsdD affect *Aspergillus flavus* morphogenesis and aflatoxin production. *Eukaryotic Cell*, *11*, 1104–1111.

Chen, E.H., Grote, E., Mohler, W. & Vignery, A. (2007) Cell-cell fusion. *FEBS Letters*, *581*, 2181–2193.

Dyer, P.S. & O'Gorman, C.M. (2012) A fungal sexual revolution: *Aspergillus* and *Penicillium* show the way. *Current Opinion in Microbiology*, *14*, 649–654.

Escaño, C.S., Juvvadi, P.R., Jin, F.J., Takahashi, T., Koyama, Y., Yamashita, S., et al. (2009) Disruption of A*opex11-1* gene involved in peroxisome proliferation leads to impaired Woronin body formation in *Aspergillus oryzae*. *Eukaryotic Cell*, *8*, 296–305.

Fischer, M.S., Wu, V.W., Lee, J.E., O'Malley, R.C., & Glass, N.L. (2018) Regulation of Cell-to-cell communication and cell wall integrity by a network of MAP kinase pathways and transcription factors in *Neurospora crassa*. *Genetics*, *209*, 489–506.

Fleißner, A. & Herzog, S. (2016) Signal exchange and integration during self-fusion in filamentous fungi. *Seminars in Cell and Developmental Biology*, *57*, 76–83.

Fleißner, A., Simonin, A.R. & Glass, N.L. (2008) Cell fusion in the filamentous fungus, *Neurospora crassa*. *Methods in Molecular Biology*, *475*, 21–38.

Fu, C., Iyer, P., Herkal, A., Abdullah, J., Stout, A. & Free, S.J. (2011) Identification and characterization of genes required for cell-to-cell fusion in *Neurospora crassa*. *Eukaryotic Cell*, *10*, 1100–1109.

Gibbons, J.G., Salichos, L., Slot, J.C., Rinker, D.C., McGary, K.L., King, J.G., et al. (2012) The evolutionary imprint of domestication on genome variation and function of the filamentous fungus *Aspergillus oryzae*. *Current Biology*, *22*, 1403–1409.

Herzog, S., Schumann, M.R. & Fleißner, A. (2015) Cell fusion in *Neurospora crassa*. *Current Opinion in Microbiology*, *28*, 53–59.

Horn, B.W., Moore, G.G. & Carbone, I. (2009) Sexual reproduction in *Aspergillus flavus*. *Mycologia*, *101*, 423–429.

Ichinomiya, M., Motoyama, T., Fujiwara, M., Takagi, M., Horiuchi, H. & Ohta, A. (2002) Repression of *chsB* expression reveals the functional importance of class IV chitin synthase gene *chsD* in hyphal growth and conidiation of *Aspergillus nidulans*. *Microbiology*, *148*, 1335–1347.

Jin, F.J., Watanabe, T., Juvvadi, P.R., Maruyama, J., Arioka, M. & Kitamoto, K. (2007) Double disruption of the proteinase genes, *tppA* and *pepE*, increases the production level of human lysozyme by *Aspergillus oryzae*. *Applied Microbiology and Biotechnology*, *76*, 1059–1068.

Jonkers, W., Fischer, M.S., Do, H.P., Starr, T.L. & Glass, N.L. (2016) Chemotropism and cell fusion in *Neurospora crassa* relies on the formation of distinct protein complexes by HAM-5 and a novel protein HAM-14. *Genetics*, *203*, 319–334.

Jonkers, W., Leeder, A.C., Ansong, C., Wang, Y., Yang, F., Starr, T.L., et al. (2014) HAM-5 functions as a MAP kinase scaffold during cell fusion in *Neurospora crassa*. *PLoS Genetics*, *10*, e1004783.

Jun, S.C., Lee, S.J., Park, H.J., Kang, J.Y., Leem, Y.E., Yang, T.-H., et al. (2011) The MpkB MAP kinase plays a role in post-karyogamy processes as well as in hyphal anastomosis during sexual development in *Aspergillus nidulans*. *Journal of Microbiology*, *49*, 418–430.

Katayama, T., Nakamura, H., Zhang, Y., Pascal, A., Fujii, W., Maruyama, J.I., et al. (2019) Forced Recycling of AMA1-based genome-editing plasmid allows for efficient multiple gene deletion/integration in the industrial filamentous fungus *Aspergillus oryzae*. *Applied and Environmental Microbiology*, *85*, e01896-18.

Kitamoto, K. (2002) Molecular biology of the *Koji* molds. *Advances in Applied Microbiology*, *51*, 129–153.

Leeder, A.C., Jonkers, W., Li, J. & Glass, N.L. (2013) Early colony establishment in *Neurospora crassa* requires a MAP kinase regulatory network. *Genetics*, *195*, 883–898.

Li, D., Bobrowicz, P., Wilkinson, H.H. & Ebbole, D.J. (2005) A mitogen-activated protein kinase pathway essential for mating and contributing to vegetative growth in *Neurospora crassa*. *Genetics*, *170*, 1091–1104.

Ma, H., Sun, X., Wang, M., Gai, Y., Chung, K.R. & Li, H. (2016) The citrus postharvest pathogen *Penicillium digitatum* depends on the PdMpkB kinase for developmental and virulence functions. *International Journal of Food Microbiology*, *236*, 167–176.

Mabashi, Y., Kikuma, T., Maruyama, J., Arioka, M. & Kitamoto, K. (2006) Development of a versatile expression plasmid construction system for *Aspergillus oryzae* and its application to visualization of mitochondria. *Bioscience, Biotechnology, and Biochemistry*, *70*, 1882–1889.

Maruyama, J. & Kitamoto, K. (2011) Targeted gene disruption in *koji* mold *Aspergillus oryzae*. *Methods in Molecular Biology*, *765*, 447–456.

Merlini, L., Dudin, O. & Martin, S.G. (2013) Mate and fuse: how yeast cells do it. *Open Biology*, *3*, 130008.

Meyer, V., Wanka, F., van Gent, J., Arentshorst, M., van den Hondel, C.A. & Ram, A.F. (2011) Fungal gene expression on demand: an inducible, tunable, and metabolism-independent expression system for *Aspergillus niger*. *Applied and Environmental Microbiolology*, *77*, 2975–2983.

Mori, N., Katayama, T., Saito, R., Iwashita, K. & Maruyama, J. (2019) Inter-strain expression of sequence-diverse HET domain genes severely inhibits growth of *Aspergillus oryzae*. *Bioscience, Biotechnology, and Biochemistry*, *83*, 1557–1569.

Morita, H., Hatamoto, O., Masuda, T., Sato, T. & Takeuchi, M. (2007) Function analysis of *steA* homolog in *Aspergillus oryzae*. *Fungal Genetics and Biology*, *44*, 330–338.

Nolting, N. & Poggeler, S. (2006) A STE12 homologue of the homothallic ascomycete *Sordaria macrospora* interacts with the MADS box protein MCM1 and is required for ascosporogenesis. *Molecular Microbiology*, *62*, 853–868.

Pandey, A., Roca, M.G., Read, N.D. & Glass, N.L. (2004) Role of a mitogen-activated protein kinase pathway during conidial germination and hyphal fusion in *Neurospora crassa*. *Eukaryotic Cell*, *3*, 348–358.

Paoletti, M., Seymour, F.A., Alcocer, M.J.C., Kaur, N., Calvo, A.M., Archer, D.B., et al. (2007) Mating type and the genetic basis of self-fertility in the model fungus *Aspergillus nidulans*. *Current Biology*, *17*, 1384–1389.

Park, G., Xue, C., Zhang, L., Lam, S. & Xu, J.R. (2002) *MST12* regulates infectious growth but not appressorium formation in the rice blast fungus *Magnaporthe grisea*. *Molecular Plant-Microbe Interactions*, *15*, 183–192.

Priegnitz, B.E., Brandt, U., Pahirulzaman, K.A.K., Dickschat, J.S. & Fleißner, A. (2015) The AngFus3 mitogen-activated protein kinase controls hyphal differentiation and secondary metabolism in *Aspergillus niger*. *Eukaryotic Cell*, *14*, 602–615.

Rispail, N. & Di Pietro, A. (2009) *Fusarium oxysporum* Ste12 controls invasive growth and virulence downstream of the Fmk1 MAPK cascade. *Molecular Plant-Microbe Interactions*, *22*, 830–839.

Rispail, N. & Di Pietro, A. (2010) The homeodomain transcription factor Ste12: connecting fungal MAPK signaling to plant pathogenicity. *Communicative and Integrative Biology*, *3*, 327–332.

Rispail, N., Soanes, D.M., Ant, C., Czajkowski, R., Grünler, A., Huguet, R., et al. (2009) Comparative genomics of MAP kinase and calcium-calcineurin signalling components in plant and human pathogenic fungi. *Fungal Genetics and Biology*, *46*, 287–298.

Rowlands, R.T. & Turner, G. (1973) Nuclear and extranuclear inheritance of oligomycin resistance in *Aspergillus nidulans*. *Molecular and General Genetics*, *126*, 201–216.

Shevchenko, A., Tomas, H., Havli, J., Olsen, J.V. & Mann, M. (2006) In-gel digestion for mass spectrometric characterization of proteins and proteomes. *Nature Protocols*, *1*, 2856–2860.

Tanaka, A., Kamiya, S., Ozaki, Y., Kameoka, S., Kayano, Y., Saikia, S., et al. (2020) A nuclear protein NsiA from *Epichloë festucae* interacts with a MAP kinase MpkB and regulates the expression of genes required for symbiotic infection and cell fusion. *Molecular Microbiology*, *114*(4), 626–640.

Tsukasaki, W., Maruyama, J. & Kitamoto, K. (2014) Establishment of a new method to quantitatively evaluate hyphal fusion ability in *Aspergillus oryzae*. *Bioscience, Biotechnology, and Biochemistry*, *78*, 1254–1262.

Vallim, M.A., Miller, K.Y. & Miller, B.L. (2000) *Aspergillus* SteA (sterile12-like) is a homeodomain-C_2/H_2-Zn^{+2} finger transcription factor required for sexual reproduction. *Molecular Microbiology*, *36*, 290–301.

Wong Sak Hoi, J. & Dumas, B. (2010) Ste12 and Ste12-like proteins, fungal transcription factors regulating development and pathogenicity. *Eukaryotic Cell*, *9*, 480–485.

Wong Sak Hoi, J., Herbert, C., Bacha, N., O'Connell, R., Lafitte, C., Borderies, G., et al. (2007) Regulation and role of a STE12-like transcription factor from the plant pathogen *Colletotrichum lindemuthianum*. *Molecular Microbiology*, *64*, 68–82.

Xiong, Y., Coradetti, S.T., Li, X., Gritsenko, M.A., Clauss, T., Petyuk, V., et al. (2014) The proteome and phosphoproteome of *Neurospora crassa* in response to cellulose, sucrose and carbon starvation. *Fungal Genetics and Biology*, *72*, 21–33.

Xu, J.R. & Hamer, J.E. (1996) MAP kinase and cAMP signaling regulate infection structure formation and pathogenic growth in the rice blast fungus *Magnaporthe grisea*. *Genes & Development*, *10*, 2696–2706.

Zhao, X., Spraker, J.E., Bok, J.W., Velk, T., He, Z.M. & Keller, N.P. (2017) A cellular fusion cascade regulated by LaeA is required for sclerotial development in *Aspergillus flavus*. *Frontiers in Microbiology*, *8*, 1925.

SUPPORTING INFORMATION

Additional Supporting Information may be found online in the Supporting Information section.

How to cite this article: Katayama T, Bayram Ö, Mo T, et al. Novel Fus3- and Ste12-interacting protein FsiA activates cell fusion-related genes in both Ste12-dependent and -independent manners in Ascomycete filamentous fungi. *Mol Microbiol*. 2021;115:723–738. https://doi.org/10.1111/mmi.14639